

## 8 Three-Phase Systems

### 8.1

#### Introduction

*Three-phase reactions* comprise gas–liquid–solid and gas–liquid–liquid reactions. Gas–liquid reactions using solid catalysts represent a very important class of reactions. Conventionally, they are carried out in slurry reactors, (bubble columns, stirred tanks), fluidized beds, fixed bed reactors (trickle beds with cocurrent downflow or cocurrent upflow, segmented bed, and countercurrent gas–liquid arrangements) and structured (catalytic wall) reactors.

For gas–liquid–liquid reactions equipment similar to that used for liquid–liquid reactions are employed. The hydrodynamics in these reactors is extremely complex because of the three phases and their convoluted interactions. An example is the “grazing” behavior of small solid particles enhancing mass transfer at gas–liquid interfaces. The scale-up from laboratory to the production site thus poses numerous problems with respect to the reactant’s mixing, temperature control (heat removal), catalyst selectivity, and its deactivation [1]. The performance of such processes can be predicted analytically only to a limited extent for reactors with well-defined flow patterns.

In this chapter, different types of microstructured devices for three-phase reactions are described. The characterization of mass transfer for gas–liquid–solid systems is presented. Finally, literature examples of both gas–liquid–solid and gas–liquid–liquid reactions are briefed.

### 8.2

#### Gas–Liquid–Solid Systems

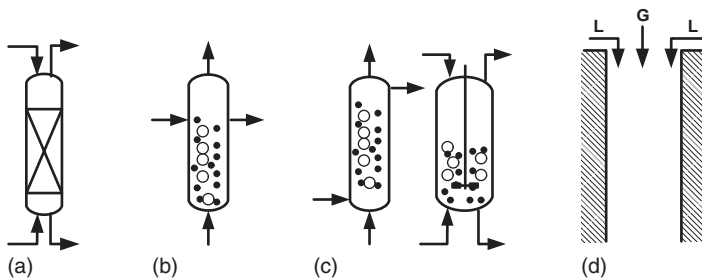
##### 8.2.1

#### Conventional Gas–Liquid–Solid Reactors

The gas–liquid–solid reactions are carried out in various types of reactors, such as packed beds, fluidized/slurry, and catalytic wall reactors (Figure 8.1). The advantages and limitations of these reactors are described in Table 8.1. Compared to fluid–solid systems, an additional phase makes it difficult to predict flow patterns

**Table 8.1** Different types of gas–liquid–solid reactors, their advantages, and limitations.

Reactors	Advantages	Limitations
Packed bed reactor (trickle bed reactor)	Easy to operate Can accommodate more than 60 (volumetric) catalyst Suitable for slow reactions	Flow maldistribution High pressure drop Risk of hot spot formation Thermal instabilities
Fluidized bed reactor	Good heat and mass transfer Pressure drop independent of fluid throughput	Good performance in the limited range of flow rates Complex hydrodynamics Broad residence time distribution Catalyst abrasion
Slurry reactor	Effective utilization of catalyst Good liquid–solid mass transfer  Good heat transfer	Moderate gas–liquid mass transfer Catalyst separation is difficult and a filtration step is required Low conversion and selectivity in continuous mode following backmixing
Catalytic wall reactors	Effective utilization of catalyst following structuring Low pressure drop	Heat/mass transfer limits the performance for fast reaction for large diameter reactors

**Figure 8.1** Schematics of Conventional reactors used for gas–liquid–solid reactions: (a) packed bed, (b) fluidized bed, (c) slurry reactor (bubble and agitated), (d) film reactor (catalytic wall).

because of their convoluted interactions. In conventional fixed bed reactors, catalyst particles of various sizes are randomly distributed, which may lead to inhomogeneous flow patterns. Near the reactor walls, the packing density is lower than the mean value, and faster flow of the fluid near the wall is unavoidable. As a result, reactants may by-pass the catalyst particles, and the residence time distribution will be broadened. Moreover, the nonuniform access of reactants to the catalytic surface diminishes the overall reactor performance and can lead to unexpected hot spots and even to reactor runaway in the case of exothermic reactions.

Pressure drop in three-phase packed beds, and thus energy consumption, is a crucial matter in process economics, in particular when large quantities of raw

materials have to be converted. On the other hand, when reactions are conducted in suspensions such as in fluidized beds or slurry reactors, pressure drop is minimized, but catalyst abrasion and catalyst recovery are critical issues.

Fluidized beds give relatively higher performance, but within a narrow operating window. Another type of reactors, the slurry reactor, effectively utilizes the catalyst because of their small particle size in the micrometer range. However, catalyst separation is difficult and a filtration step is required to separate fine particles from the product. Moreover, when applied in the continuous mode, backmixing lowers the conversion and usually the selectivity [2]. Conventional continuous tubular reactors are used as falling film or wall reactor with catalyst coated on the wall; however, supply/removal of heat and often broad residence time distribution because of large reactor diameters are two main drawbacks commonly encountered with such reactors.

Structured catalysts may be used to overcome the drawbacks of conventional catalytic reactors [3]. These are reactors with monolithic converters, with catalyst-coated static mixers and arranged packings as applied in distillation and absorption columns.

### 8.2.2

#### Microstructured Gas–Liquid–Solid Reactors

Different types of gas–liquid–solid microstructured reactors (MSR) have been developed, using different gas–liquid contacting principles [4]. These principles can be classified as

- Continuous phase contacting, where the fluid phases are separated. Examples are microstructured falling film and mesh reactors.
- Dispersed phase contacting that is obtained when one of the fluid phases is dispersed into the other phase.

##### 8.2.2.1 Continuous Phase Microstructured Reactors

In *falling film contactors* a thin film is created by a liquid falling under gravity pull. The liquid flows over a solid support (see Figure 8.2), which is normally a thin wall or stack of pipes. In conventional falling film devices, a film with a thickness of 0.5–3 mm is generated [4]. This rather thick liquid film results in an important mass transfer resistance for the gaseous reactant diffusing to the solid catalyst on the reactor wall. In addition, the film flow becomes unstable at high throughput and the film may break up into rivulets, fingers or a series of droplets. The mentioned problems can be overcome by microstructuring the solid wall [5, 6]. The microstructured falling film reactor consists of microchannels, which are typically 300  $\mu\text{m}$  wide, 100  $\mu\text{m}$  deep, and about 80 mm long. The channels are separated by 100  $\mu\text{m}$  wide walls. The microstructured falling film reactor has been described in detail in the previous chapter.

In a *mesh microcontactors*, the gas and liquid flow through separate channels. To provide stable operation the fluids are separated by a thin mesh of typically 5  $\mu\text{m}$  thickness. The fluids are in contact through holes with diameters of about

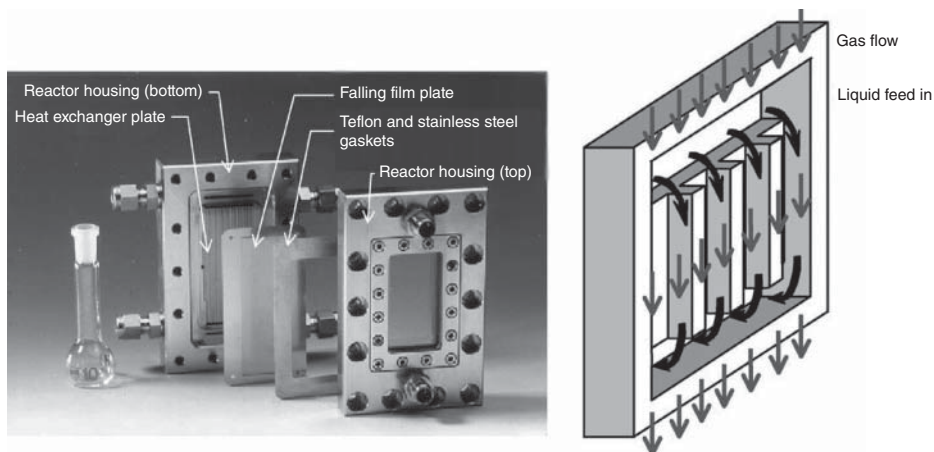


**Figure 8.2** Components and schematic of the microstructured falling film reactor [7]. (Adapted with permission from Elsevier.)

5  $\mu\text{m}$  [8]. In contrast to microstructured falling film reactors, the velocity of the fluids can be varied without changing the interfacial area, which is given by the porosity of the membrane. Interfacial forces help to stabilize the fluid interface within the openings, while fluid layers are thin enough to enhance mass transfer.

The meniscus shape at the interface between the two phases defines the available area for mass transfer and is a function of contact angle, pore geometry, and pressure difference between phases. The open area of the micromesh contactor can be as high as 40% while the mesh to wall distances can be set, generally, to 80–140  $\mu\text{m}$  providing chamber volumes of  $\sim 100 \mu\text{l}$ . A quadrant-reactor configuration with a deep outlet channel at the circumference provides radial flow and minimizes flow resistances ensuring even the flow of the fluidic streams (and consequently residence time) in the reactor (see Figure 8.3). The mesh is fabricated in nickel using a two-stage electroplating method. It is placed between two glass layers that form the chambers for the two fluids. The struts that help preserve the physical structure of the mesh fabricated on the mesh align with pillars on the glass to provide the necessary channel width of the reactant channels. For gas–liquid–solid reactions, the bottom glass insert in the reaction chamber can be coated with a catalytic layer.

#### 8.2.2.2 Dispersed Phase Microstructured Reactors

In gas–liquid systems (Chapter 7) different flow regimes for two phase systems are observed. One of the most stable and commonly applied flow regime in which one fluid flow in the form of dispersed phase is segmented (Taylor) flow. Taylor flow is characterized by gas bubbles that are too large to retain a spherical shape and are deformed to fit inside the channel. Surface tension provides the driving force for the bubbles to attain a spherical shape, and the bubbles try to expand toward the channel wall such that only a thin film of liquid remains between the

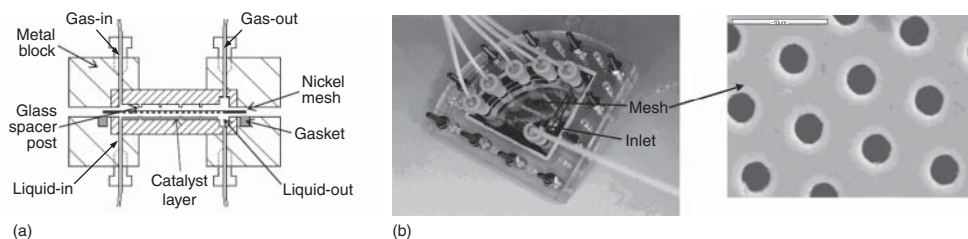


**Figure 8.3** Mesh microcontactor.

(a) Schematics of mesh contactors. (Adapted from Ref. [8]. With permission of The Royal Society of Chemistry.) (b) Fully assembled

micromesh reactor and microstructured mesh. (Adapted with permission from Ref. [4]. Copyright (2005) American Chemical Society.)

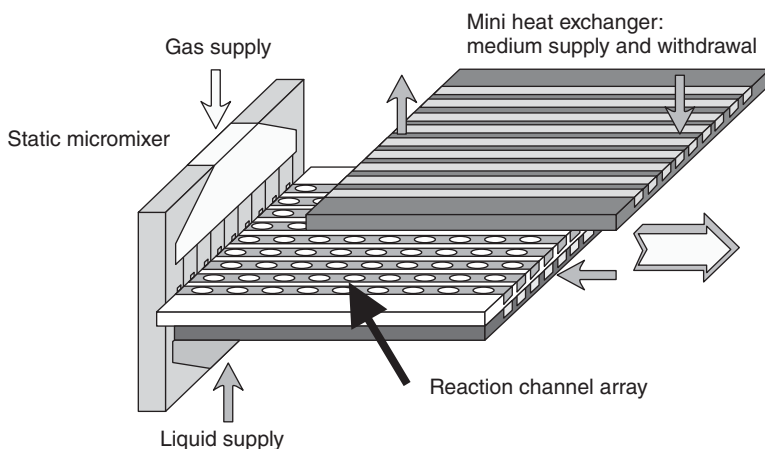


**Figure 8.4** Microbubble column with integrated cooling channels. (Reproduced from Ref. [9]. With kind permission of Springer Science + Business Media.)

gas and the wall. The liquid slugs are entrapped between the bubbles. This flow regime is also used for three phase reactions.

In *segmented flow gas-liquid-solid reactors*, the liquid usually flows over the solid surface while the gas flows through the liquid in the form of bubbles or annular flow (see Figure 8.4), depending on the MSR geometry and the catalyst arrangement.

The hydrodynamic characteristics of these reactors, such as pressure drop and residence time distribution, can be determined from those for fluid-solid and fluid-fluid reactors. The difference between the gas-liquid and gas-liquid-solid systems is that because of the reaction at the surface of the catalyst, there is always a concentration gradient in the liquid phase in the latter case.

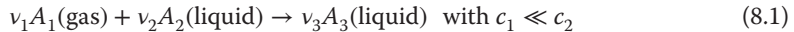
*Microstructured packed beds* have been used for gas-liquid-solid reactions. An advantage of microstructured packed beds for heterogenous catalytic processes stems from the fact that active and selective catalysts are commercially

available. In addition, the particle size of these catalysts used in suspension reactors is in the micrometer range and fit well for use in microchannels. However, a proper design of the reactor is required to maintain an acceptable pressure drop. To avoid an excessive pressure drop, an MSR consisting of a microfluidic distribution manifold and a microchannel array were constructed [10]. Multiple reagent streams (specifically, gas and liquid streams) were mixed on-chip, and the fluid streams were brought into contact by a series of interleaved, high-aspect-ratio inlet channels. These inlet channels deliver the reactants continuously and concurrently to 10 reactor chambers containing standard catalytic particles in the diameter range of 50–75  $\mu\text{m}$ .

### 8.2.2.3 Mass Transfer and Chemical Reaction

The global transformation rate of a gas–liquid reaction catalyzed by a solid catalyst is influenced by the mass transfer between the gas–liquid and the liquid–solid. The two mass transfer processes and the surface reaction are in series and for fast chemical reactions, mass transfer will influence the reactant concentration on the catalytic surface and, as a consequence, influence the reactor performance and the product selectivity. Compared to gas–solid catalytic reactions as discussed in Section 2.5, an additional resistance in the liquid must be considered (Figure 8.5).

The general discussion of the reaction in gas–liquid–solid systems is based on the simple film model. In addition, we consider an irreversible reaction between a gaseous reactant ( $A_1$ ) and a reactant in the liquid phase ( $A_2$ ), which is in large excess:



If the thickness of the catalytic layer on the reactor wall is sufficiently small, internal mass transfer resistances can be neglected and only external resistances in the fluid phases are considered. The reaction rate per unit of the outer surface of the catalytic layer is described by a pseudo first order reaction ( $\text{mol m}^2 \text{s}^{-1}$ ):

$$r_s = k_s c_{1,s} \quad \text{with : } c_{2,s} = c_{2,L} \gg c_{1,s} \quad (8.2)$$

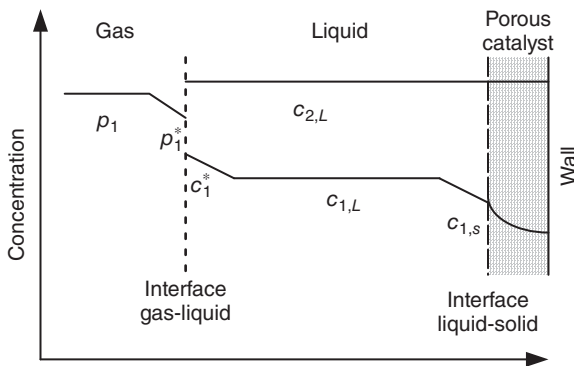


Figure 8.5 Concentration profiles of reactants in the gas, liquid, catalyst phase.

The reaction rate per unit volume of the liquid (continuous) phase is given as

$$r = k_s a_{LS} c_{1,s} = k c_{1,s} \quad (8.3)$$

where  $a_{LS}$  corresponds to the interfacial liquid/solid area:  $a_{LS} = A_{LS}/V_L$ .

The mass transfer rate ( $r_m$ ) from the liquid phase to the surface of the catalytic layer is proportional to the concentration gradient between the two phases:

$$r_{m,LS} = k_{LS} a_{LS} (c_{1,L} - c_{1,s}) \quad (8.4)$$

The rate of the volumetric mass transfer ( $r_m$ ) from gas phase to liquid is proportional to the overall concentration gradient between the two phases:

$$r_{m,GL} = k_{GL} a_{GL} \left( \frac{p_1}{H} - c_{1,L} \right) \quad (8.5)$$

where  $H$  is the Henry constant,  $p_1$  is the partial pressure of  $A_1$  in the bulk gas phase,  $k_{GL}$  is the overall gas/liquid mass transfer coefficient, and  $a_{GL}$  corresponds to the specific gas/liquid interfacial area referred to the liquid phase  $a_{GL} = A_{GL}/V_L$ .

Under stationary conditions the reaction rate and mass transfer rates must be identical:  $r_{m,LS} = r_{m,GL} = r$ . From Equations 8.5 and 8.3 follows:

$$\begin{aligned} k c_{1,s} &= k_{LS} a_{LS} (c_{1,L} - c_{1,s}) \\ \Rightarrow c_{1,s} &= \frac{k_{LS} a_{LS}}{k_{LS} a_{LS} + k} c_{1,L} = \frac{1}{1 + DaII_{LS}} c_{1,L}; \quad DaII_{LS} = \frac{k}{k_{LS} a_{LS}} \end{aligned} \quad (8.6)$$

Here  $DaII_{LS}$  is the ratio of reaction rate constant to the liquid–solid mass transfer coefficient. Similarly, the relation between gas and liquid phase concentrations can be established by equating Equations 8.4 and 8.5 as

$$\begin{aligned} k_{GL} a_{GL} \left( \frac{p_1}{H} - c_{1,L} \right) &= k_{LS} a_{LS} (c_{1,L} - c_{1,s}) \\ \Rightarrow c_{1,L} &= \frac{k_{GL} a_{GL}}{k_{GL} a_{GL} + k_{LS} a_{LS} - \frac{(k_{LS} a_{LS})^2}{k_i + k_{LS} a_{LS}}} \left( \frac{p_1}{H} \right) \end{aligned} \quad (8.7)$$

Finally, the concentration at the catalyst surface can be calculated as function of the partial pressure of the gaseous reactant  $A_1$  with Equations 8.6 and 8.7:

$$c_{1,s} = \frac{1}{1 + \frac{k}{k_{GL} a_{GL}} + \frac{k}{k_{LS} a_{LS}}} \left( \frac{p_1}{H} \right) = \frac{1}{1 + DaII_{GL} + DaII_{LS}} \left( \frac{p_1}{H} \right) \quad (8.8)$$

The observed (effective) reaction rate follows:

$$r_{s,\text{eff}} = \frac{k}{1 + DaII_{GL} + DaII_{LS}} \left( \frac{p_1}{H} \right) \quad (8.9)$$

If we consider a microstructured falling film reactor, the liquid phase is reduced to a small liquid layer between the gas phase and the solid catalyst as shown schematically in Figure 8.6a. The thickness of this film ( $\delta_{\text{film}}$ ) depends on the liquid flow as discussed in Chapter 7. Because of the surface forces the wetting liquids form a meniscus within the channel. With increasing flow rate the meniscus becomes more and more flat. This is demonstrated on Figure 8.6b for a channel with a width of 300  $\mu\text{m}$  and a height of the side walls of 100  $\mu\text{m}$  [11]. The channel

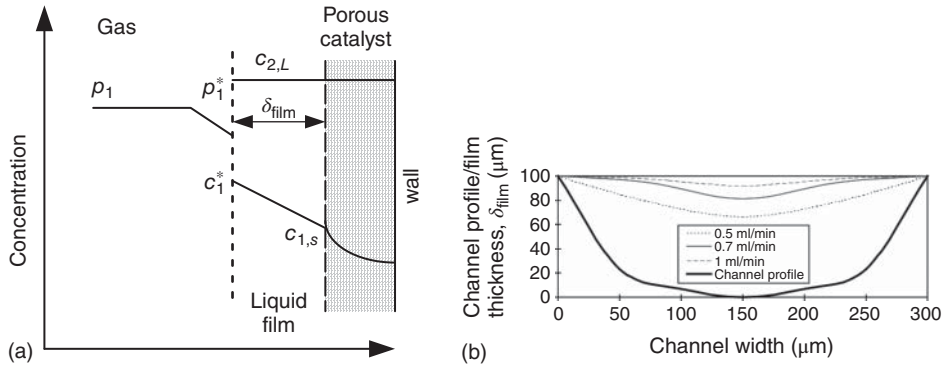


**Figure 8.6** (a) Concentration profile in a catalytic microstructured film reactor (schematic) and (b) average liquid film thickness profile across a channel at various flowrates [11] (Adapted with permission from Elsevier.)

profile itself is also curved because of the procedure of catalyst coating. In spite of the observed radial film profile, which depends on the fluid and solid properties the average film thickness will be estimated based on the simple Nusselt falling film theory given in Equation 8.10 (Chapter 7).

$$\delta_{\text{film}} = \sqrt[3]{\frac{3\dot{V}_L v_L}{n \cdot W \cdot g \cdot \sin \theta} \frac{\rho_L}{(\rho_L - \rho_G)}} \cong \sqrt[3]{\frac{3\dot{V}_L v_L}{n \cdot W \cdot g \cdot \sin \theta}}; \delta_{\text{film}} \leq H \quad (8.10)$$

where  $\theta$  is an inclination angle from horizontal and  $g$  is the gravitational acceleration.

As flow rate increases, the liquid film thickness increases up to the maximum value given by the height of the channel walls. An increase in film thickness will increase the diffusion time for solutes across the liquid film to the catalyst surface, thus increasing the mass transfer resistance and decreasing the effective reaction rate and diminish the conversion. Higher flow rates will decrease the mean residence time of the fluid, thus reducing the conversion as well.

An eventual influence of the reactant diffusion in the porous catalytic layer can be respected by adding an efficiency factor  $\eta$  to the rate constant (see Chapter 2), and the observed reaction rate is given by Equation 8.11.

$$r_{\text{ob}} = \frac{1}{\frac{1}{k_{\text{GL}} a_{\text{GL}}} + \frac{1}{k_{\text{LS}} a_{\text{LS}}} + \frac{1}{\eta k}} \left( \frac{p_1}{H} \right) = \frac{\eta k}{1 + \frac{\eta k}{k_{\text{GL}} a_{\text{GL}}} + \frac{\eta k}{k_{\text{LS}} a_{\text{LS}}}} \left( \frac{p_1}{H} \right) \quad (8.11)$$

In many practical situations, the main mass transfer resistance is concentrated in the liquid phase and the mass transfer resistance in the gas phase can be neglected. The mass transfer coefficient in the liquid film can be estimated based on the film model to be:

$$k_{\text{LS}} = \frac{D_m}{\delta_{\text{film}}} \quad (8.12)$$



The specific interfacial area ( $a_{LS}$ ) can be estimated as

$$a_{LS} = \frac{\text{Interfacial surface area}}{\text{liquid volume}} \cong \frac{W \cdot L}{\delta_{\text{film}} \cdot W \cdot L} = \frac{1}{\delta_{\text{film}}} \quad (8.13)$$

The estimations of film thickness and mass transfer coefficient are demonstrated in Example 8.1.

**Example 8.1: Film thickness and mass transfer coefficient of falling film MSR.**

Estimate the film thickness, mass transfer coefficient, volumetric mass transfer coefficient, and specific interfacial area for a vertically placed falling film MSR with the dimensions:  $W = 600 \mu\text{m}$ ,  $H = 200 \mu\text{m}$ ,  $L = 100 \text{ mm}$ . The liquid flow rate is fixed to  $\dot{V}_L = 0.1 \text{ cm}^3 \text{ min}^{-1}$   $0.1 \text{ ml/min}$ .

Data:  $\rho_L = 1000 \text{ kg m}^{-3}$ ,  $\nu_L = 10^{-6} \text{ m}^2 \text{ s}^{-1}$ ,  $D_m = 10^{-9} \text{ m}^2 \text{ s}^{-1}$ ,  $n = 5$

**Solution:**

The film thickness is estimated using Nusselt falling film theory given by Equation 8.10.

$$\delta_{\text{film}} \cong \sqrt[3]{\frac{3\dot{V}_L \cdot \nu_L}{n \cdot W \cdot g \cdot \sin \theta}} = \sqrt[3]{\frac{3 \cdot \left(\frac{0.1 \cdot 10^{-6}}{60}\right) \cdot 1 \cdot 10^{-6}}{5 \cdot (1 \cdot 10^{-3}) \cdot 9.81 \cdot \sin(90)}} = 46.7 \mu\text{m}$$

Mass transfer coefficient ( $k_{LS}$ ) and specific interfacial area ( $a_{LS}$ ) given by Equation 8.12:

$$k_{LS} = \frac{D_m}{\delta_{\text{film}}} = \frac{1 \cdot 10^{-9}}{46.7 \cdot 10^{-6}} = 2.14 \cdot 10^{-5} \text{ m} \cdot \text{s}^{-1}$$

$$a_{LS} \cong \frac{1}{\delta_{\text{film}}} = \frac{1}{46.7 \cdot 10^{-6}} = 2.1 \cdot 10^4 \text{ m}^2 \cdot \text{m}^{-3}$$

Thus, the volumetric mass transfer coefficient is

$$k_{LS}a_{LS} = 2.14 \cdot 10^{-5} \times 2.1 \cdot 10^4 = 0.45 \text{ s}^{-1}$$

From the above example, it is clear that the specific interfacial area and thus the volumetric mass transfer coefficients are high in falling film reactors and are suitable for fast catalytic reactions.

In a *mesh microcontactor*, the meniscus shape at the interface between the two phases defines the available area for mass transfer and is a function of contact angle, pore geometry, and pressure difference between phases. The open area of the micromesh contactor can be as high as 40%, which leads to gas-liquid interfacial area of  $2000 \text{ m}^2 \text{ m}^{-3}$ . This high gas-liquid interfacial area combined with the small fluid layer thickness in the order of  $100 \mu\text{m}$  results in high mass transfer coefficients. The volumetric mass transfer coefficient reported for the very fast

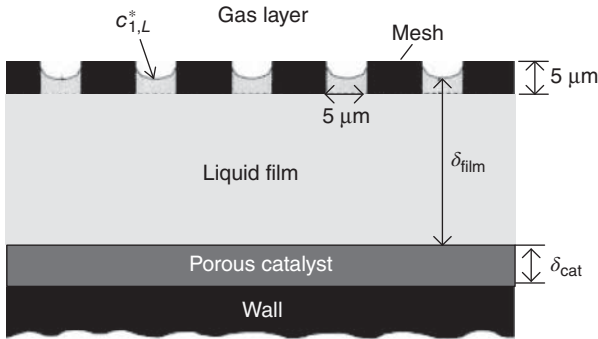


**Figure 8.7** Mesh reactor (schematic) [12]. (Adapted with permission from Wiley.)

hydrogenation of  $\alpha$ -methylstyrene over a Pd/ $\gamma$ -alumina catalyst was found to be in the range of  $0.8\text{--}1.6\text{ s}^{-1}$  [12, 13] (Figure 8.7).

In *segmented flow gas–liquid–solid reactors*, the liquid usually flows over the solid surface while the gas flows through the liquid in the form of bubbles or annular flow, depending on the channel geometry and the catalyst arrangement.

The hydrodynamic characteristics of the three-phase reactors, such as pressure drop and residence time distribution, can be determined from those for fluid–solid and fluid–fluid reactors.

For the gaseous reactant three mass transfer steps can be identified [14]: (i) the transfer from the bubble through the liquid film to the catalyst ( $k_{GS}a_{GS}$ ), (ii) the transfer from the caps of the gas bubbles to the liquid slug ( $k_{GL}a_{GL}$ ), and (iii) the transfer of dissolved gas to the catalytic surface ( $k_{LS}a_{LS}$ ). Steps (ii) and (iii) are in series and in parallel with respect to step (i) (Figure 8.8).

The overall resistance using resistances in series and parallel can be written as

$$\frac{1}{R_{ov}} = \frac{1}{R_{GS}} + \frac{1}{R_{GL} + R_{LS}} \quad (8.14)$$

Replacing the resistance with volumetric mass transfer coefficients, the following expression can be obtained for overall volumetric mass transfer ( $k_{ov}a$ ):

$$k_{ov}a = k_{GS}a_{GS} + \frac{1}{\frac{1}{k_{GL}a_{GL}} + \frac{1}{k_{LS}a_{LS}}} \quad (8.15)$$

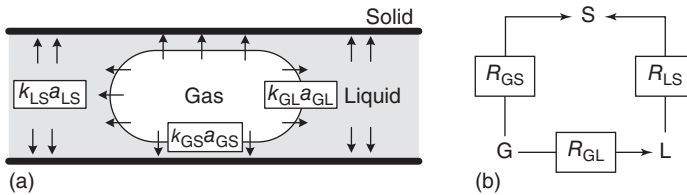


**Figure 8.8** Mass transfer in dispersed phase microstructured reactors where gas solute diffuses through liquid toward solid surface. (a) Schematic representation. (b) Resistance model.

Various attempts were made to determine the individual mass transfer coefficients in Equation 8.15 in nonreactive systems. However, because the concentration profiles in the liquid surface film and in the slugs are strongly affected by fast chemical reactions, caution must be exercised in extending the results to reactive systems.

The mass transfer resistance through the caps of the bubble and the liquid phase are particularly difficult to estimate as assured models are missing. The transfer from the gas bubble through the wall film can be estimated. Ignoring the thickness of the film, the specific interfacial area is given by

$$a_{GS} = \frac{4}{d_t} \epsilon_G \quad (8.16)$$

with  $\epsilon_G$  the volume fraction of the gas phase.

The mass transfer resistance is given mainly by the diffusion through the thin wall film. With the film model we obtain:

$$k_{GS} = \frac{D_m}{\delta_{\text{film}}} \quad (8.17)$$

The film thickness can be estimated with the relations presented in Chapter 7 [15, 16].

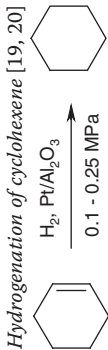
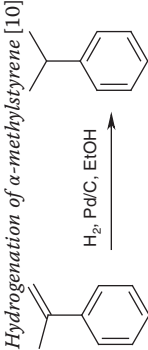
$$\begin{aligned} \delta_{\text{film}} &= 0.67 d_t Ca_L^{2/3} \quad \text{for } Ca_L \leq 3 \cdot 10^{-3} \\ \delta_{\text{film}} &= d_t \frac{0.67 Ca_L^{2/3}}{1 + 3.35 Ca_L^{2/3}} \quad \text{for } Ca_L < 1 \end{aligned} \quad (8.18)$$

The mass transfer model presented in Equation 8.15 was applied to interpret experimental results characterizing the hydrogenation of 4-nitrobenzoic acid to 4-aminobenzoic acid [17]. The reaction was conducted in a capillary with a circular cross section and a washcoat incorporating an alumina-supported palladium catalyst. Flow regimes in the microreactor were characterized visually for different flow rates and gas to liquid flow ratios. For low liquid and gas velocities, bubbles were formed at the entrance and were carried by the liquid through the packed bed. Under these conditions the hydrogenation of cyclohexene was studied and used as a model reaction to measure the mass transfer resistances. Overall, mass transfer coefficients ( $k_{ov}a$ ) were measured in the range of 5 to 15 s<sup>-1</sup>, which is nearly 2 orders of magnitude larger than values reported in the literature for standard laboratory-scale reactors [18].

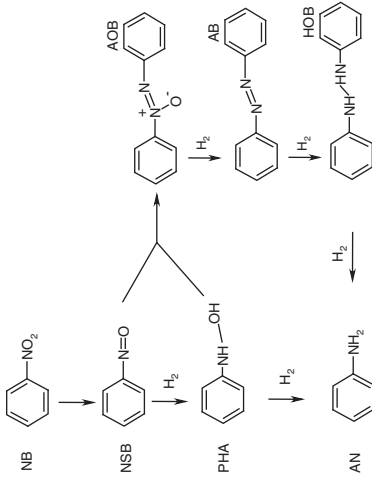
#### 8.2.2.4 Reaction Examples

Most of the reported microstructured gas-liquid-solid reactors concern catalytic hydrogenations (Table 8.2). This is because hydrogenation reactions represent about 20% of all the reaction steps in a typical fine chemical synthesis. Catalytic hydrogenations are fast and highly exothermic reactions. Consequently, reactor performance and product selectivity are strongly influenced by mass transfer, and heat evacuation is an important issue. Both problems may be overcome using microstructured devices.

**Table 8.2** Reaction examples, types of reactions, and results obtained in gas–liquid–solid reactions.

Reaction/example	Type of reactor	Performance/yield/selectivity
<p><i>Hydrogenation of cyclohexene</i> [19, 20]</p> 	Packed bed MSR (catalyst powder different sizes: 53–75, 36–38, or <36 μm)	Improved mass transfer (~10 s <sup>-1</sup> ) over its macroscale counterpart (100-fold)
<p><i>Hydrogenation of α-methylstyrene</i> [10]</p> 	Packed bed MSR	Conversion 20–100%  The initial reaction rates ~0.01 mol min <sup>-1</sup> per channel – favorable compared with the intrinsic kinetics in the literature [21]
<i>Hydrogenation of cyclohexene</i> [20]	Channels with staggered column	Mass transfer coefficients 3–7 s <sup>-1</sup>  Initial reaction rates 6.5 × 10 <sup>-5</sup> mol min <sup>-1</sup> m <sup>-2</sup> with the porous silicon support vs 4.5 × 10 <sup>-5</sup> mol min <sup>-1</sup> m <sup>-2</sup> with the powdered catalyst

## Hydrogenation of nitrobenzene to aniline [7]



Falling film reactor

MSR 394 kmol aniline  $\text{m}^{-3}$  reactor (NB –  $0.1 \text{ mol l}^{-1}$ , temperature  $60^\circ\text{C}$ , pressure 1 bar) while a batch reactor 204 kmol aniline  $\text{m}^{-3}$  reactor (NB  $0.4 \text{ mol l}^{-1}$ , temperature  $125^\circ\text{C}$ , pressure 20 bar)

Hydrogenation of *p*-nitrotoluene [22, 23]

Channel MSR

Conversion varied from 58 to 98% (370K, 2MPa)

Similar conversion to conventional fixed bed but better heat removal

Hydrogenation of  $\alpha$ -methylstyrene [4, 13]

Mesh MSR

Mass transfer coefficient  $1 - 2 \text{ s}^{-1}$

In the gas–liquid–solid MSR, catalyst is incorporated either as a packed bed or as a coating. In the packed bed reactors, standard porous catalysts are incorporated and the fluid streams are brought into contact. In the falling film MSR, the catalyst is incorporated as thin nonporous films or as particles in alumina-coated walls [4].

A microstructured film reactor was used for the hydrogenation of nitrobenzene (NB) to aniline (AN) in ethanol at 60 °C, 0.1–0.4 MPa hydrogen pressure and residence time of 9–17 s [7, 11]. Palladium catalyst was deposited as films or particles on the microstructured plate. Confocal microscopy was used to measure the liquid film thickness. With increasing flow rates between 0.5 and 1.0 cm<sup>3</sup> min<sup>-1</sup> thicker liquid films between 67 and 92 μm were observed. The  $k_L a$  of this system was estimated to be 3–8 s<sup>-1</sup> with an interfacial surface area per reaction volume of 9000–15 000 m<sup>2</sup> m<sup>-3</sup>. Conversion was found to be affected by both liquid flow rate and hydrogen pressure, and the reactor operated between the kinetic and mass transfer controlled regimes.

Many reported MSR used for gas–liquid–solid reactions are *micro packed beds*. An advantage of microstructured packed bed for hydrogenation processes stems from the fact that active and selective catalysts are commercially available.

Gas–liquid–solid reactions, mainly hydrogenations, studied in the literature are summarized in Table 8.2. A micro packed bed reactor (Figure 8.9) to carry out the hydrogenation of cyclohexene, a model reaction for multiphase reactors, over standard platinum supported on alumina powder (platinum content was either 1 or 5 wt%) [19, 20]. Gas and liquid inlet flows are split among several channels that deliver the reactants continuously and cocurrently to 10 reaction chamber. A wide channel perpendicular to these small channels is used to deliver the catalyst slurry to the reaction chamber, which is filtered at the end. The small particles provide the high surface areas for improved gas–liquid mixing but they also represent a challenge in terms of pressure drop and fluid distribution among the 10 parallel channels.

To avoid packing variations, Jensen [24] and Losley *et al.* [19] formed regular posts within silicon channels as shown in Figure 8.10. These posts can be rendered catalytically active by surface treatment or, for example, by coating with alumina and subsequent impregnation with platinum [25].

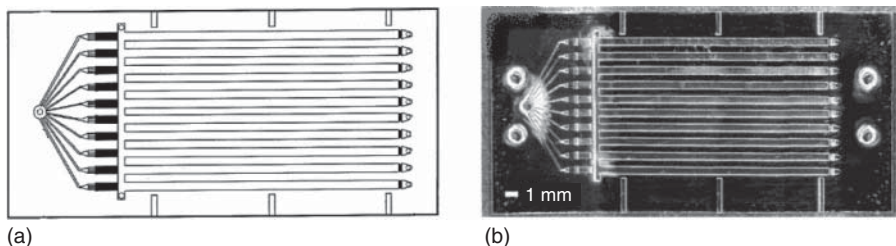


**Figure 8.9** Packed bed MSR. (a) Top silicon layer illustrating fluid manifold to 10 parallel fixed bed reaction channels. (b) Photomicrograph of multichannel reactor chip. (Adapted with permission from Ref. [20]. Copyright (2001) American Chemical Society.)

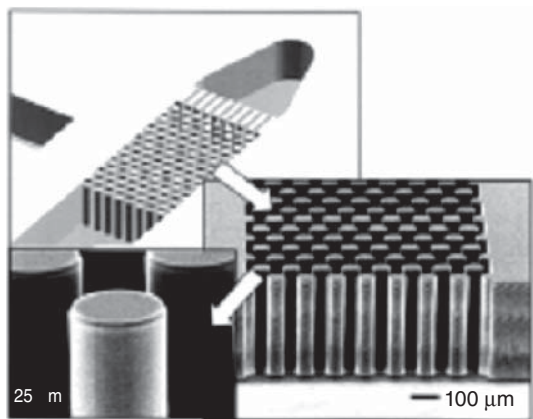


**Figure 8.10** Microfabricated structured catalyst packing inside a microchannel [24]. (Adapted with permission from Elsevier.)

A microstructured falling film reactor was used for hydrogenation of NB to AN ( $\Delta H_r = -545 \text{ kJ mol}^{-1}$ ) in ethanol [7]. The reaction can proceed along different pathways and involved several intermediates, which can also react with each other and can be controlled by precise temperature. The catalyst, palladium, was deposited as films or particles via sputtering, UV decomposition of palladium acetate, or incipient wetness impregnation. The results show that such reaction is feasible in the falling film MSR provided that suitable catalyst incorporation methods are employed. The deactivation of catalyst was observed through the formation of organic compounds on the catalyst surface and palladium loss. Among all,  $\gamma$ -alumina-supported palladium prepared through incipient wetness impregnation was found to be reasonably robust.

A mesh reactor was used for heterogenous hydrogenation of  $\alpha$ -methylstyrene to cumene [13]. Two catalysts  $\text{Pd}/\text{Al}_2\text{O}_3$  and  $\text{Pt}/\text{Al}_2\text{O}_3$  were used. The activity of the catalyst is too high resulting in mass transfer limitations. A global volumetric mass transfer coefficient of ( $1-2 \text{ s}^{-1}$ ) was roughly estimated applying “in series mass transfer resistances concept” [20] and considering a fast first order reaction that are in the range of those found in commercial pressure reactors.

A channel MSR without any internals for mixing can also be used for three-phase reactions: hydrogenation of *p*-nitrotoluene to *p*-toluidine in microchannel reactors using different ways of preparation of the Pd catalyst [22]. Practically this reaction is free of by-products, that is, selectivity to *p*-toluidine is 100%. Depending on the operating conditions, the conversion was varied from 58 to 98% in MSR. The conversion for an electrodeposited palladium was 58%, for chemical deposited palladium was in between 58 and 98%, for impregnated catalyst on an electro-oxidized nanoporous substrate was 89%, and for fixed bed catalyst was 85%. Though the best MSR conversion is similar to that of a conventional fixed bed reactor, the increased heat removal allowed a pronounced decrease in reaction time down to some few minutes [23].

Increasing flow velocities in the microreactor lead to pulsations and the formation of segmented flow. The different flow pattern observed in microstructured packed beds were studied in detail [26]. They confirm the segregated flow pattern at high gas fractions. More recently, the catalytic hydrogenation of *o*-nitroanisole in a microstructured packed bed reactor was studied [27]. The reactor had an inner diameter of 0.775 mm and was filled with Pd/zeolite catalyst with particle diameter in the range of 45–75 and 75–150  $\mu\text{m}$ . The length of the catalytic bed could be varied between 60 and 80 mm. It is stated that segmented gas–liquid flow was observed, but, further hydrodynamic studies are missing.

To increase mass transfer in solid catalyzed gas–liquid hydrogenations, the reactions are often operated at high pressures. Silicon/glass MSR present a possibility to safely handle high pressure and provide optical access into the reaction channel for flow investigations. A Si/glass MSR with soldered microfluidic connections for high pressure and high temperature applications was used [28]. Mechanical testing of the device by tensile and pressure tests showed no failure for continuous operation at 14 MPa and 80 °C. The MSR design is applied for the well-described solid catalyzed exothermic hydrogenation of cyclohexene at operating conditions up to 5.1 MPa and 71 °C.

### 8.3

#### Gas–Liquid–Liquid Systems

Gas–liquid–liquid reactions have several applications such as hydroformylation, carbonylation, hydrogenation, oligomerization, polymerization, hydrometallurgical applications, biochemical processes, and fine chemicals manufacturing. Developments in homogenous catalysis have made these reaction systems increasingly attractive in recent years. Gas–liquid–liquid systems are encountered in reaction systems that comprise three phases of two (or more) immiscible reactants, reaction products, or catalyst [29]. In some cases, the three reactants are supplied from three different phases (e.g., Koch reaction). It is also possible to intensify the mass transfer in a liquid–liquid system; additional gas phase may be added to enhance mixing and augment the interfacial area.

The reactors that are used for gas–liquid and liquid–liquid applications (Chapter 7) can be applied to gas–liquid–liquid system with a provision to add an additional fluid. The flow patterns of gas–liquid–liquid flow in the MSR depend on the volume fraction of each phase within the reactor. At low gas volume fractions, the gas remains in one of the liquids while both liquids flow in the form of slugs. If the reaction is mass transfer limited, the overall reaction rate is strongly dependent on the interfacial liquid–liquid mass transfer. By reducing the capillary diameter, the specific interfacial area increases and leads to an intensified process.

A selective hydrogenation of  $\alpha$ ,  $\beta$ -unsaturated aldehydes in aqueous solution was carried out using PTFE capillary of diameter from 500 to 1000  $\mu\text{m}$  [30]. The gas–liquid–liquid flow observed in the reactor is depicted in Figure 8.11. It shows



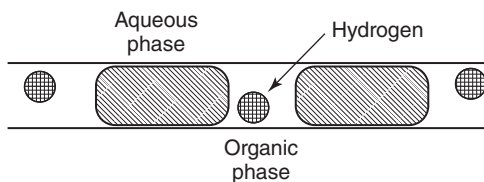


**Figure 8.11** Schematics of gas–liquid–liquid flow patterns observed in the selective hydrogenation of  $\alpha$ ,  $\beta$ -unsaturated aldehydes. (Adapted with permission from Wiley.)

the alternate flow of two liquid phases with the organic phase forming a wall film because of its affinity toward the capillary material and hydrogen in the form of small bubbles. The reaction rate showed a significant effect of global reaction rates with a threefold increase by reducing the channel diameter from 1000 to 500  $\mu\text{m}$ .

## 8.4

### Summary

In this chapter, characterization of mass transfer for gas–liquid–solid systems in MSR has been described.

The readers are advised to read the previous chapter for understanding some of the aspects that are just briefed here. The mass transfer models for both continuous phase and dispersed phase MSR are discussed in detail. From the mass transfer and chemical reaction expressions it was found that the investigation of the contribution of each term is possible only with certain assumption.

Gas–liquid–liquid systems are encountered in reaction systems that comprise three phases of two (or more) immiscible reactants, reaction products, or catalyst. The reactors that are used for such reactions are similar to gas–liquid and liquid–liquid applications with a provision to add an additional fluid. The flow patterns of gas–liquid–liquid flow in the MSR depend on the volume fraction of each phase within the reactor.

Finally, the reaction examples presented in the literature are briefed.

## 8.5

### List of Symbols

$a_{LS}, a_{GL}, a_{GS}$	Liquid/solid specific interfacial area, gas/liquid specific interfacial area, gas/solid specific interfacial area	$\text{m}^2 \text{m}^{-3}$
$c_s$	Concentration at catalytic surface	$\text{mol m}^{-3}$
$c^*$	Equilibrium concentration	$\text{mol m}^{-3}$
$p^*$	Equilibrium pressure	Pa
$k_s$	Rate constant in the catalytic reaction where reaction rate is defined per unit catalytic layer	Variable

$R_{GS}, R_{GL}, R_{LS}$	Resistance in gas–solid mass transfer, in gas–liquid mass transfer, in liquid–solid mass transfer, overall	s
$R_{ov}$		
$r_m$	Mass transfer rate	$\text{mol m}^{-3} \text{s}^{-1}$
$r_s$	Reaction rate per unit of the catalytic layer	$\text{mol m}^{-2} \text{s}^{-1}$
$\delta_{\text{film}}$	Thickness of the film	m
$\theta$	Inclination angle from horizontal in falling film reactor	°
$\eta$	Efficiency factor	—

## References

- Shah, Y.T. (1979) *Gas liquid Solid Reactor Design*, McGraw-Hill, New York.
- Pangarkar, K., Schildhauer, T.J., Van Ommen, J.R., Nijenhuis, J., Kapteijn, F., and Moulijn, J.A. (2008) Structured packings for multiphase catalytic reactors. *Ind. Eng. Chem. Res.*, **47** (10), 3720–3751.
- Cybulski, A. and Moulijn, J.A. (eds) (2006) *Structured Catalysts and Reactors*, 2nd edn, Taylor & Francis Group, Boca Raton, FL, London, New York.
- Hessel, V., Angeli, P., Gavriilidis, A., and Lowe, H. (2005) Gas-liquid and gas-liquid-solid microstructured reactors: contacting principles and applications. *Ind. Eng. Chem. Res.*, **44** (25), 9750–9769.
- Hessel, V., W. Ehrfeld, Herweck, T., Haverkamp, V., Löwe, H., Schiewe, J., Wille, C., Kern, T., and Lutz, N. (2000) *Proceedings of the 4th International Conference on Microreaction Technology (IMRET 4)*, AIChE, Atlanta, pp. 174–186.
- Jähnisch, K., Baerns, M., Hessel, V., Ehrfeld, W., Haverkamp, V., Löwe, H., Wille, C., and Guber, A. (2000) Direct fluorination of toluene using elemental fluorine in gas/liquid microreactors. *J. Fluorine Chem.*, **105** (1), 117–128.
- Yeong, K.K., Gavriilidis, A., Zapf, R., and Hessel, V. (2003) Catalyst preparation and deactivation issues for nitrobenzene hydrogenation in a microstructured falling film reactor. *Catal. Today*, **81** (4), 641–651.
- Wenn, D.A., Shaw, J.E.A., and Mackenzie, B. (2003) A mesh micro-contactors for 2-phase reactions. *Lab Chip*, **3**, 180–186.
- Hessel, V., Ehrfeld, W., Golbig, K., Haverkamp, V., Löwe, H., Storz, M., and Wille, C. (1999) in *Proceedings of the 3rd International Conference on Microreaction Technology (IMRET3)* (ed. W. Ehrfeld), Springer, Berlin, p. 526.
- Losey, M.W., Schmnidt, M.A., and Jensen, K.F. (eds) (2000) *International Conference on Microreaction Technology (IMRET 3)*, Springer-Verlag, Frankfurt, pp. 277–286.
- Yeong, K.K., Gavriilidis, A., Zapf, R., and Hessel, V. (2004) Experimental studies of nitrobenzene hydrogenation in a microstructured falling film reactor. *Chem. Eng. Sci.*, **59** (16), 3491–3494.
- Abdallah, R., Magnico, P., Fumey, B., and De Bellefon, C. (2006) CFD and kinetic methods for mass transfer determination in a mesh microreactor. *AIChE J.*, **52** (6), 2230–2237.
- Abdallah, R., Meille, V., Shaw, J., Wenn, D., and De Bellefon, C. (2004) Gas-liquid and gas-liquid-solid catalysis in a mesh microreactor. *Chem. Commun.*, **10** (4), 372–373.
- Kreutzer, M.T., Du, P., Heiszwolf, J.J., Kapteijn, F., and Moulijn, J.A. (2001) Mass transfer characteristics of three-phase monolith reactors. *Chem. Eng. Sci.*, **56** (21-22), 6015–6023.
- Aussillous, P. and Quere, D. (2000) Quick deposition of a fluid on the wall of a tube. *Phys. Fluids*, **12** (10), 2367–2371.

16. Bretherton, F.P. (1961) The motion of long bubbles in tubes. *J. Fluid Mech.*, **10** (2), 166–188.
17. Tsoiligkas, A.N., Simmons, M.J.H., and Wood, J. (2007) Two phase gas-liquid reaction studies in a circular capillary. *Chem. Eng. Sci.*, **62**, 5397–5401.
18. De Bellefon, C., Lamouille, T., Pestre, N., Bornette, F., Pennemann, H., Neumann, F., and Hessel, V. (2005) Asymmetric catalytic hydrogenations at micro-litre scale in a helicoidal single channel falling film micro-reactor. *Catal. Today*, **110** (1-2), 179–187.
19. Losey, M.W., Jackman, R.J., Firebaugh, S.L., Schmidt, M.A., and Jensen, K.F. (2002) Design and fabrication of microfluidic devices for multiphase mixing and reaction. *J. Microelectromech. Syst.*, **11** (6), 709–717.
20. Losey, M.W., Schmidt, M.A., and Jensen, K.F. (2001) Microfabricated multiphase packed-bed reactors: characterization of mass transfer and reactions. *Ind. Eng. Chem. Res.*, **40** (12), 2555–2562.
21. Herskowitz, M., Carbonell, R.G., and Smith, J.M. (1979) Effectiveness factors and mass transfer in trickle-bed reactors. *AIChE J.*, **25** (2), 272–283.
22. Födisch, R., Hönicke, D., Xu, Y., and Platzer, B. (2001) *International Conference on Microreaction Technology (IMRET 5)*, Strasbourg, Berlin, Springer-Verlag, pp. 470–478.
23. Reschetilowski, W. and Hönicke, D. (1999) Heterogeneously catalyzed liquid-phase hydrogenation of nitro-aromatics using microchannel reactors. *DGMK Tagungsbericht*, **9903**, 231–238.
24. Jensen, K.F. (2001) Microreaction engineering – is small better? *Chem. Eng. Sci.*, **56** (2), 293–303.
25. Meille, V., Pallier, S., Santa Cruz, Bus-tamante G.V., Roumanie, M., and Reymond, J.-P. (2005) Deposition of -Al<sub>2</sub>O<sub>3</sub> layers on structured supports for the design of new catalytic reactors. *Appl. Catal. Gen.*, **286** (2), 232–238.
26. van Herk, D., Kreutzer, M.T., Makkee, M., and Moulijn, J.A. (2005) Scaling down trickle bed reactors. *Catal. Today*, **106** (1-4), 227–232.
27. Tadepalli, S., Haider, R., and Lawal, A. (2007) Catalytic hydrogenation of o-nitroanisole in a microreactor: reactor performance and kinetic studies. *Chem. Eng. Sci.*, **62** (10), 2663–2678.
28. Trachsel, F., Hutter, C., and von Rohr, P.R. (2008) Transparent silicon/glass microreactor for high-pressure and high-temperature reactions. *Chem. Eng. J.*, **135** (Suppl. 1), S309–S316.
29. Kaur, R., Machiraju, R., and Nigam, K.D.P. (2007) Agitation effects in a gas-liquid-liquid reactor system: methyl ethyl ketazine production. *Int. J. Chem. Reactor Eng.*, **5**, 1–19.
30. Önal, Y., Lucas, M., and Claus, P. (2005) Application of a capillary microreactor for selective hydrogenation of  $\alpha,\beta$ -unsaturated aldehydes in aqueous multiphase catalysis. *Chem. Eng. Technol.*, **28** (9), 972–978.